

PACS Classification: 79.20.Hx, 82.53.Ps, 61.80.-x

ELECTRON CASCADES PRODUCED BY PHOTOELECTRONS IN DIAMOND

Beata Ziaja^{y,z}, Abraham Szöke^{y,x}, Janos Hajdu¹

Department of Biochemistry, Biomedical Centre, Box 576, Uppsala University, S-75123 Uppsala, Sweden

^y Department of Theoretical Physics, Institute of Nuclear Physics, Radzikowskiego 152, 31-342 Cracow, Poland

^z High Energy Physics, Uppsala University, P.O. Box 535, S-75121 Uppsala, Sweden

^x Lawrence Livermore National Laboratory, Livermore, CA 94551, USA

Corresponding author:

Janos Hajdu, Department of Biochemistry, Biomedical Centre,
Box 576, Uppsala University, S-75123 Uppsala, Sweden
Tel:+4618 4714449, Fax:+4618 511755, E-mail:hajdu@xray.bmc.uu.se

Abstract: Secondary electron cascades are responsible for significant ionizations in macroscopic samples during irradiation with X-rays. A quantitative analysis of these cascades is needed, e.g. for assessing damage in optical components at X-ray free-electron lasers, and for understanding damage in samples exposed to the beam. Here we present results from Monte Carlo simulations, showing the space-time evolution of secondary electron cascades in diamond. These cascades follow the impact of a single primary electron at energies between 0.5–12 keV, representing the usual range for photoelectrons. The calculations describe the secondary ionizations caused by these electrons, the three-dimensional evolution of the electron cloud, and monitor the equivalent instantaneous temperature of the free-electron gas as the system cools during expansion. The dissipation of the impact energy proceeds predominantly through the production of secondary electrons whose energies are comparable to the binding energies of the valence (40–50 eV) and the core electrons (300 eV) in accordance with experiments and the models of interactions. The electron cloud generated by a 12 keV electron is strongly anisotropic in the early phases of the cascade ($t \leq 1$ fs). At later times, the sample is dominated by low energy electrons, and these are scattered more isotropically by atoms in the sample. The results show that

¹e-mail: ziaja@tsl.uu.se, szoke1@llnl.gov, hajdu@xray.bmc.uu.se

the emission of secondary electrons approaches saturation within about 100 fs, following the primary impact. At an impact energy of 12 keV, the total number of electrons liberated in the sample is ~ 400 at 1000 fs. The results provide an understanding of ionizations by photoelectrons, and extend earlier models on low-energy electron cascades ($E = 0.25$ keV, [1, 2]) to the higher energy regime of the photoelectrons.

In atomic or molecular samples exposed to X-ray radiation damage occurs. In light elements it proceeds mainly via the photoelectric effect. Photoelectrons and Auger electrons [3] are then emitted. They propagate through the sample, and cause further damage by excitations of secondary electrons. Photoelectrons released by X-rays of ~ 1 Å wavelength (~ 12 keV) are fast, $v \sim 660$ Å/fs, and they can escape from small samples early in an exposure. In contrast, Auger electrons are slow ($v \sim 95$ Å/fs in carbon), so they remain longer in a sample, and it is likely that they will thermalize there. An analysis of electron cascades initiated by Auger electrons in diamond is described in [2].

A detailed description of electron cascades initiated by an electron impact of energy between 0.5 – 12 keV is needed for a better understanding of radiation damage in larger samples as secondary ionization caused by propagating photoelectrons is significant there. Such processes need to be investigated for planned experiments with free-electron-lasers (FEL). Atomic and molecular clusters irradiated with VUV radiation have already been studied experimentally [4].

Energetic photoelectrons ($E > 0.5$ keV in carbon) propagate almost freely through the medium. They interact with single atoms, and this interaction is well described by the Born approximation [5, 6]. Here, we use the formalism of the Lindhard dielectric function [7] together with two optical models (the TPP-2 and Ashley's models [8–13]) to describe the inelastic interactions of electrons with atoms. This approach takes into account the valence and core ionizations of an atom, following the inelastic scattering of a free electron. This approximation works well for energies up to about 10 keV, and in this energy regime core ionization are responsible for not more than about 10 % of the total number of ionizations in solids [14].

In this paper elastic scattering is treated in the muffin-tin potential approximation [1, 2, 5, 6]. In previous studies on low-energy electrons (with energies up to, $E = 0.4$ keV), we used programs from the Barbieri/Van Hove Phase Shift package [15]. For electrons of energies, $E = 0.4$ keV, and higher, we obtained elastic cross sections from the NIST database [16].

Fig. 1 shows the total elastic and inelastic cross sections obtained from the calculations. The results show that for energies higher than 1 keV, the elastic and inelastic cross sections are comparable, but for lower energies, $0.1 < E < 1$ keV, the elastic cross section is twice

as large as the inelastic one. For very low energies, $E < 0.1$ keV, the inelastic cross sections drop rapidly as the energy decreases, and elastic interactions become predominant. This was true for both optical models (Ashley and TPP-2).

Fig. 2 shows the energy loss function (ELF) and the cross sections for core ionization from the K shell of carbon as estimated from the Lindhard approximation, using the optical models above. The figures were compared to results from the relativistic binary- encounter-Bethe model (RBEB) [17] for the total core ionization by impact electrons. This model was developed by combining a modified form of the Mott cross section and the leading dipole part of the Bethe cross section [18]. Recently, it was extended to incident electrons with relativistic energies [17]. When the incoming electron is fast, we can use the Bethe-Fermi approximation [19,20]. It replaces the electric field of the incoming electron by an electromagnetic pulse of the same, short duration. Impact ionization is then proportional to the dipole transition probability caused by the short, non-periodic electromagnetic pulse. Incidentally, that is the basis of the two optical models used here. The ionization probability is proportional to the overlap of the bound electron wave function with that of the secondary electron. Simple scaling considerations predict that if valence electrons are ionized, their kinetic energies should not be much larger than a few times the shell binding energy. Figure 3 shows that the mean energy of the secondary electrons in diamond is about 40-50 eV (close to the energy of L shell electrons), reaching peak energies of about 300 eV (close to the energy of core electrons). The energy loss function in Fig. 2 is the sum of the large valence and small core contributions which add to the valence contribution at energies, $E \approx 0.3$ keV. For comparison, the binding energy of the K shell in carbon is, $E_B = 285$ eV. It is difficult to separate the contribution of the core excitations from the valence excitations on the base of the ELF alone. Therefore, we make here a rough estimate of the pure core contribution by subtracting the valence component from ELF. The valence component was extrapolated at the edge of the core peak, i. e. for energies larger than 277 eV (cf. Fig. 2). The cross section obtained from this core contribution underestimates the RBEB cross section at energies smaller than $1 \approx 2$ keV. This is due to the fact that the optical approximation does not apply at the core threshold. At larger energies our estimate agrees well with the RBEB predictions. This discrepancy does not make our results inaccurate.

Fig. 3 shows the energy loss, Δ , during a single inelastic scattering of an electron on an atom as a function of the electron energy. These are the values obtained at fixed integrated probabilities, $P(\Delta \leq E) = \frac{\int_0^{\Delta} d\Delta^0(d(E)=d\Delta^0)}{\int_0^{\Delta_{max}} d\Delta^0(d(E)=d\Delta^0)}$, and represent the integrated probabilities of inelastic electron-atom scattering with the energy loss that is less or equal to Δ at the impact energy, E . The energy loss, Δ , does not exceed 0.3 keV, and its value becomes independent from the impact energy, E , at energies greater than

1 keV. This is expected as one-electron excitations are predominant in inelastic scatterings [19, 20].

Results

We performed a large set of Monte Carlo simulations in diamond, showing the path of an impact electron and the secondary electron cascade triggered by the electron. Electron trajectories were simulated as described in [2] in such a way that no energy loss was permitted to the lattice. This approximation gave a better estimate of ionization rates in [2] than the approximation where the energy loss to the lattice was allowed. The starting position of the impact electron at $t = 0$ fs was at the origin $\mathbf{x}=(0,0,0)$ of an arbitrarily chosen coordinate system, and the velocity of the impact electron was along the Z-axis. Motions of holes and ionizations by the holes were neglected since they influence the dynamics of electrons at very low electron energies only. The space-time characteristics of secondary cascades were recorded as functions of the impact energy and time.

The energy dependence of the elastic and inelastic cross sections had a strong influence on the dynamics of the electron cloud (cf. Fig. 1). At longer times, when most of the electrons have already cooled to low energies, elastic (isotropic) scatterings dominate the sample. Electrons then propagate randomly through the sample, and their distribution is isotropic. Earlier studies show similar behaviour for Auger electrons [2].

Evolution of the cascade was analysed through (a) the number of secondary ionizations, $N_{el}(t)$, and (b) the equivalent instantaneous temperature of the free electron gas $kT(t)$. Quantities (a), (b) were averaged over a number of cascades. Figure 4 shows the results obtained with Ashley's and the TPP-2 optical models for impact energies of $E = 0.5; 1.5; 5; 12$ keV. 0.5 keV corresponds to the lowest energy of an incident electron at which the Born approximation may be applied when calculating the electron-atom cross sections in carbon [21].

The number of ionization events within the first femtosecond is within 10-25 for electron impact energies of $E = 0.5 - 12$ keV. For impacts at lower energies, $E = 1.5$ keV, the number of ionizations was between 20 - 70, and saturated within 100 fs. At higher impact energies there was an increase in the number of the ionization events after $t > 100$ fs, however, the sample was then dominated by low energy electrons ($E < 20$ eV) (cf. Figs. 6), and thus not many ionizations could be expected to occur. We checked that at 1000 fs, there was a total of about 400 ionizations induced by an electron impact of 12 keV (Ashley's model), compared to 370 ionizations at 100 fs. When using the TPP-2 model, the corresponding numbers were 360 both at 100 fs and 1000 fs at 12 keV impact energy.

The equivalent instantaneous temperature of the electron gas decreased as the cascade evolved. We used this temperature equivalent since the electron gas was far from thermal equilibrium. However, the equivalent temperature is still a quantity conserved in electron-electron collisions. It is worth noticing that after 10 fs the temperature curves obtained at totally different primary energies were very similar. This indicated that the number of electrons was not much influenced by the energy of the primary electron but rather by secondary electrons of lower energies (< 60 eV) which dominated the sample after 10 fs. At 100 fs the temperature of the electron gas dropped to 5 eV (Ashley's) or 2.5 eV (the TPP-2 model).

Fig. 5 shows plots of **(a)** the average number of electrons released, N_{el} ; **(b)** the equivalent instantaneous temperature, kT , of the electron gas as a function of the energy, E , of the primary electron. These curves describe results obtained at different times ($t = 1; 10; 90$ fs), and were based on Ashley's model and on the TPP-2 model with **no** energy transfer allowed to the lattice. The data represent primary energies of $E = 0.25; 0.5; 1.5; 5; 12$ keV. Results for impact energy $E = 0.25$ keV were taken from Ref. [2]. The results can be used for the interpolation of the number of ionizations, and the temperature of the electrons at energies ranging from $E = 0.25$ keV to $E = 12$ keV.

Fig. 5 shows that the number of secondary electrons, N_{el} , is approximately proportional to the impact energy. The slight curvature of the dependence indicates that the system has not yet reached equilibrium at 90 fs after the primary impact (cf. Fig. 4).

The energy distribution of secondary electrons. The positions and velocities of electrons recorded at times, $t = 1; 10; 90$ fs at energies of $E = 0.5; 1.5; 5; 12$ keV were collected from all cascades, and put into one file. Using these data, histograms for the energy distributions were obtained, $N(E) = N$, at these time points. Number, $N(E) = \frac{1}{P} \sum_{i=1}^{500} N_i(E)$, is the average number of electrons in a bin, $(E; E + \Delta E)$, averaged over a number of cascades. Correspondingly, $N_i(E)$ was the number of electrons found in that bin for the i th cascade. These distributions were normalized to the total number of electrons, $N = \frac{1}{P} \sum_E N(E)$. Fig. 6 shows the histograms at impact energies of $E = 0.5$ keV and $E = 12$ keV. As expected, the energy histograms show that the number of low-energy electrons increased with time. One may notice that the dissipation of the impact energy was fast. At 1 fs, most electrons had energies lower than 300 eV in the cascade. This follows from the assumption that one-electron excitations dominate electron-atom interactions, and events in which energy transfer exceeds the threshold for core ionizations by a secondary electron are rare. At 10 fs most of the electrons had energy lower than 40 eV in all cascades. The overall low energy of the electrons at that time influence ionization rates and the expansion rate of the electron cloud, and these both slowed down after 10 fs. At 100 fs there were only low energy electrons ($E < 20$ eV)

present in the sample, and elastic scatterings dominated the dynamics of the electron cloud.

Spatial distribution of secondary electrons. In order to describe the spatial distribution of the secondary electron cloud in cascades triggered by $E = 0.5$ and $E = 12$ keV electrons, results from 500 simulations were analysed at these energies. Most electrons lay within a sphere whose radius depends on the electron impact energy. At 1 fs, it was $r_{\text{cloud}} = 50$ Å for 0.5 keV impact energy, and $r_{\text{cloud}} = 600$ Å for 12 keV impact energy. At 100 fs the corresponding radii were between 150 Å and 3100 Å respectively. At this time, the center of mass of the cloud moved 23–1400 Å away from the starting point in the direction of the primary impact at energies of 0.5–12 keV, respectively (Fig. 7). The shifts in other directions were small (1–33 Å).

The sphericity tensor, $S^{ab} = \frac{1}{N} \sum_{i=1}^N r_i^a r_i^b = \frac{1}{N} \sum_{i=1}^N r_i^2 \delta^{ab}$, calculated for the collective cloud was almost diagonal. Non-diagonal elements were 10^{-1} – 10^{-4} times smaller than the diagonal ones. The sphericity tensor was diagonalized, and the sphericity parameter, S , was obtained from its eigenvalues: $S = 3/(2(\lambda_1 + \lambda_2 + \lambda_3))$, where $\lambda_1 \geq \lambda_2 \geq \lambda_3$. For electron impacts of 0.5 and 12 keV S falls within the interval of 0.91–0.96 at 10 fs and 0.91–0.98 at 90 fs, suggesting that the spatial distribution of the collective cloud was practically isotropic at that stage.

Strong differences at the spatial distribution of the electron cloud manifested at 1 fs. At low impact energies (0.5 and 1.5 keV), S was within the interval of 0.8–0.9, while at 5 keV S was 0.4–0.5, and at 12 keV, S was around 0.30–0.35. This shows a strong anisotropy with increasing impact energy. The distribution of the cloud was cylindrically symmetrical along the primary impact vector but it was elongated along the direction of the impact. This is due to the fact that at 1 fs, the primary electron was much faster than the secondary electrons. At later times the sample became dominated by low energy electrons, which were scattered more isotropically. This is reflected in the progressing isotropy in the distribution.

The final cloud at higher impact energies is pear-shaped. Figure 9 gives a quantitative description of the development of such clouds, using parameters shown in Figure 8. Parameters z_+ , z_- and r represent root mean square values from 500 simulations,

$$\begin{aligned} z_+ &= \sqrt{\frac{1}{N} \sum_{i=1}^N h(z - z_{CM})^2 \mathbf{i}; z > z_{CM}} \\ z_- &= \sqrt{\frac{1}{N} \sum_{i=1}^N h(z - z_{CM})^2 \mathbf{i}; z < z_{CM}} \\ r &= \sqrt{\frac{1}{N} \sum_{i=1}^N h(x - x_{CM})^2 + (y - y_{CM})^2 \mathbf{i};} \end{aligned} \quad (1)$$

and were calculated in respect to the center of mass of the cloud. The results confirm that the cloud is elongated along the axis of the primary impact (Z) at early times, and becomes more spherical later.

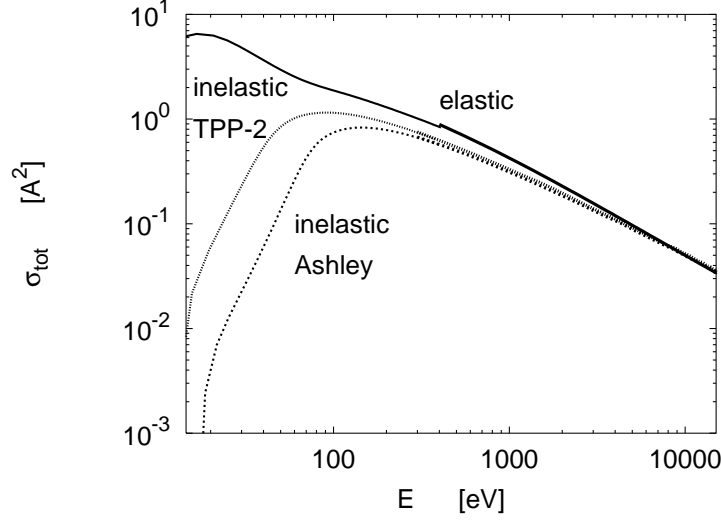


Figure 1: Elastic and inelastic total cross sections for diamond. Inelastic cross sections are obtained from the Lindhard approximation with core ionization taken into account using the TPP-2 optical model or Ashley’s optical model. Elastic cross sections up to energies, $E = 0.4$ keV, were derived with the Barbieri/Van Hove Phase Shift package [15]. For larger energies, the elastic cross sections were taken from the NIST database.

Conclusions

Our results can be used to estimate damage by photo electrons ($E = 0.5 - 12$ keV) in diamond and other carbon-based covalent compounds. The Monte-Carlo code may be adopted to simulate multiionization phenomena in different systems, ranging from the explosion of atomic clusters to the formation of warm dense matter and plasmas. The model could also be used to estimate ionization rates and the spatio-temporal characteristics of secondary electron cascades in biological substances.

Acknowledgments

We are grateful to Gyula Faigel, Zoltan Jurek, Michel A. van Hove for discussions. B. Z. thanks Peter Druck and the Institute of Theoretical Physics II at the Ruhr University in Bochum for providing the access to the computational unit. This research was supported in part by the Polish Committee for Scientific Research with grant No. 2 P03B 05119, the EU-BIOTECH Programme and the Swedish Research Councils. A. S. is grateful to STINT for a distinguished guest professorship. B. Z. was supported by the Wenner-Gren Foundations.

References

- [1] B. Ziaja, D. van der Spoel, A. Szöke, and J. Hajdu. *Phys. Rev. B*, 64:214104, 2001.
- [2] B. Ziaja, A. Szöke, D. van der Spoel, and J. Hajdu. *Phys. Rev. B*, 66:024116, 2002.
- [3] R. Neutze, R. Wouts, D. van der Spoel, E. Weckert, and J. Hajdu. *Nature*, 406:752–757, 2000.
- [4] Thomas Moeller et al. ‘Project on “Optical Non-Linear Processes, Multi-Photon Ionisation, and Coulomb Explosion of Atoms and Clusters by Intense Vacuum Ultraviolet Radiation”. *FEL, HASYLAB, DESY*, 2000-2002.
- [5] B.H. Bransden and C.J. Joachain. Physics of atoms and molecules. *Longman, Essex*, pages 505–513, 1998.
- [6] P.G. Burke. Atomic, molecular and optical physics handbook. Editor G.W.F. Drake. *Woodbury, New York American Institute of Physics*, page 536, 1996.
- [7] J. Lindhard. *K. Dan. Vidensk. Selsk. Mat. Fys. Medd.*, 28:1–57, 1954.
- [8] S. Tanuma, C.J. Powell, and D.R. Penn. *Surf. Interf. Anal.*, 11:577, 1988.
- [9] S. Tanuma, C. J. Powell, and D. R. Penn. *Surf. Interf. Anal.*, 17:911, 1991.
- [10] K. Yoshihara S. Tanuma, S. Ichimura. *Appl. Surf. Scien.*, 100/101:47, 1996.
- [11] J.C. Ashley. *J. Elec. Spec. Rel. Phenom.*, 46:199, 1988.
- [12] J.C. Ashley. *J. Elec. Spec. Rel. Phenom.*, 50:323–334, 1990.
- [13] J.C. Ashley. *J. Appl. Phys.*, 69:674, 1991.
- [14] P. Pianetta. Low-energy electron ranges in matter. *X-ray data booklet*, pages 3–5, 2001.
- [15] A. Barbieri and M.A. van Hove. private communication; Phase Shift package, <http://electron.lbl.gov/leedpack/>.
- [16] A. Jablonski and C. Powell. NIST Standard Reference Database.
- [17] Y.-K. Kim, J.P. Santos, and F. Parente. *Phys. Rev. A*, 62:052710, 2000.
- [18] Y.-K. Kim and M.E. Rudd. *Phys. Rev. A*, 50:3954, 1994.
- [19] E. Fermi. *Z. Phys.*, 29:315, 1924.

[20] H. Bethe. *Ann. Phys. (Leipzig)*, 5:325, 1930.

[21] J.M. Fernández-Varea et al. *Nucl. Inst. Meth. Phys. Res. B*, 108:35–50, 1996.

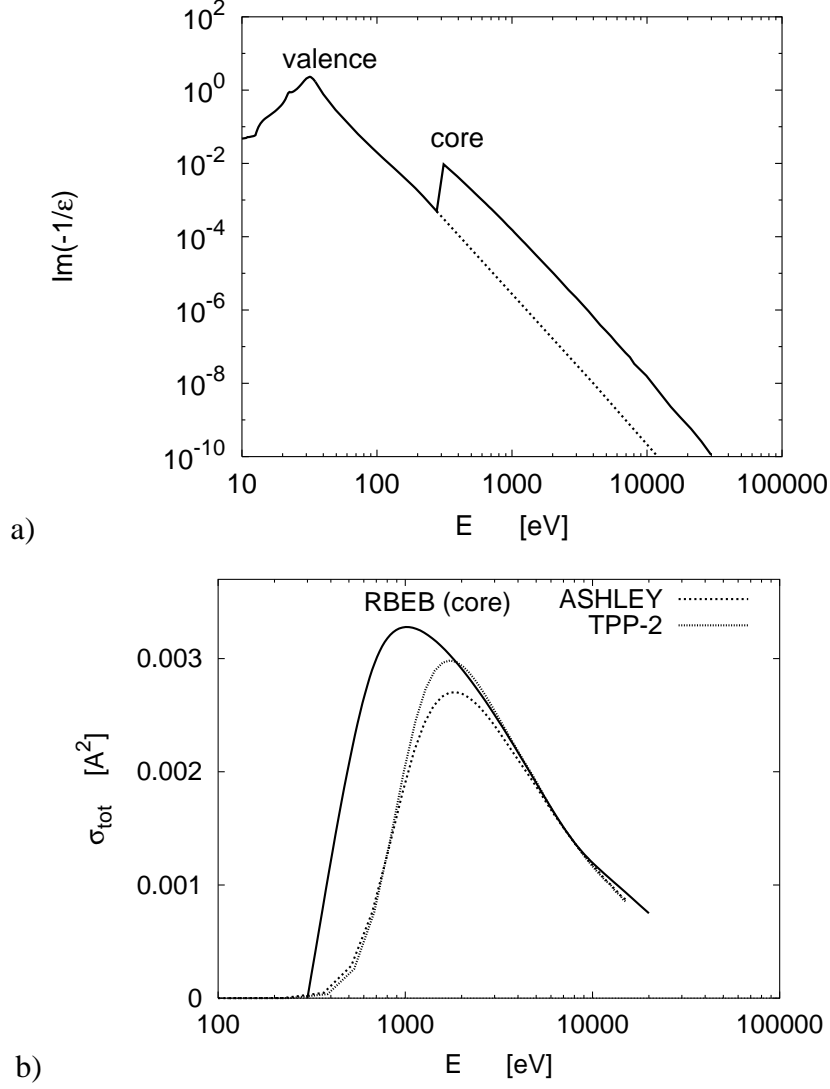


Figure 2: (a) Energy loss function of diamond, $\text{Im}(-1/\epsilon)$, and (b) the total cross section for core ionization of diamond. Results from the Lindhard approximation, obtained with Ashley's and the TPP-2 models are compared to the prediction of RBEB model for core ionization from K shell in carbon [17]. The binding energy of a K shell electron in carbon is, $E_B = 285$ eV.

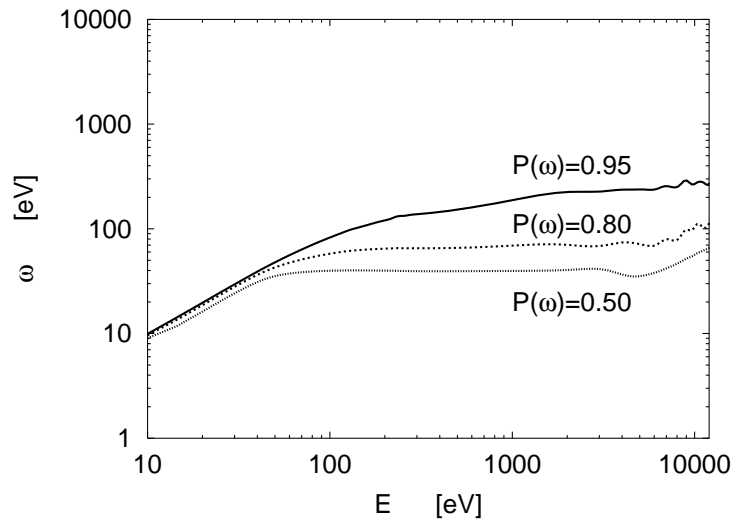


Figure 3: Energy loss, ω , in a single inelastic scattering event during electron-atom interactions in diamond as a function of electron energy. Plots show results at fixed integrated probabilities, $P(\omega \leq E) = 0.5; 0.8; 0.95$, obtained with the TPP-2 model. The probability $P(\omega \leq E)$ is the integrated probability that the energy loss in a scattering is less or equal ω . Results from Ashley's model were very similar (not shown)

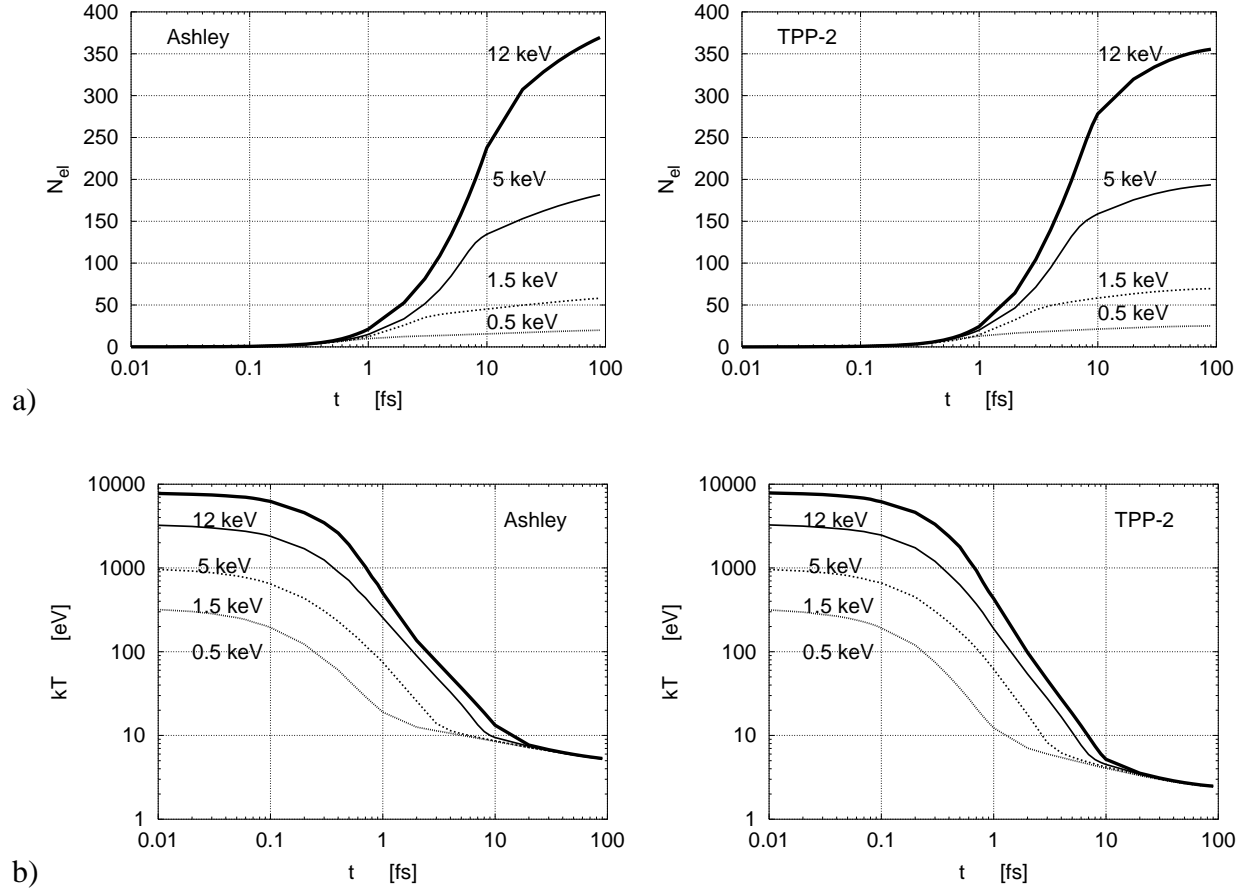


Figure 4: **(a)** Average number of secondary electrons emitted, N_{el} , vs. time; **(b)** The equivalent instantaneous temperature kT of electron gas vs. time averaged over 500 cascades. Curves correspond to the results obtained at different electron impact energies $E = 0.5 - 12$ keV from Ashley's model and the TPP-2 model with **no** energy transfer allowed to the lattice.

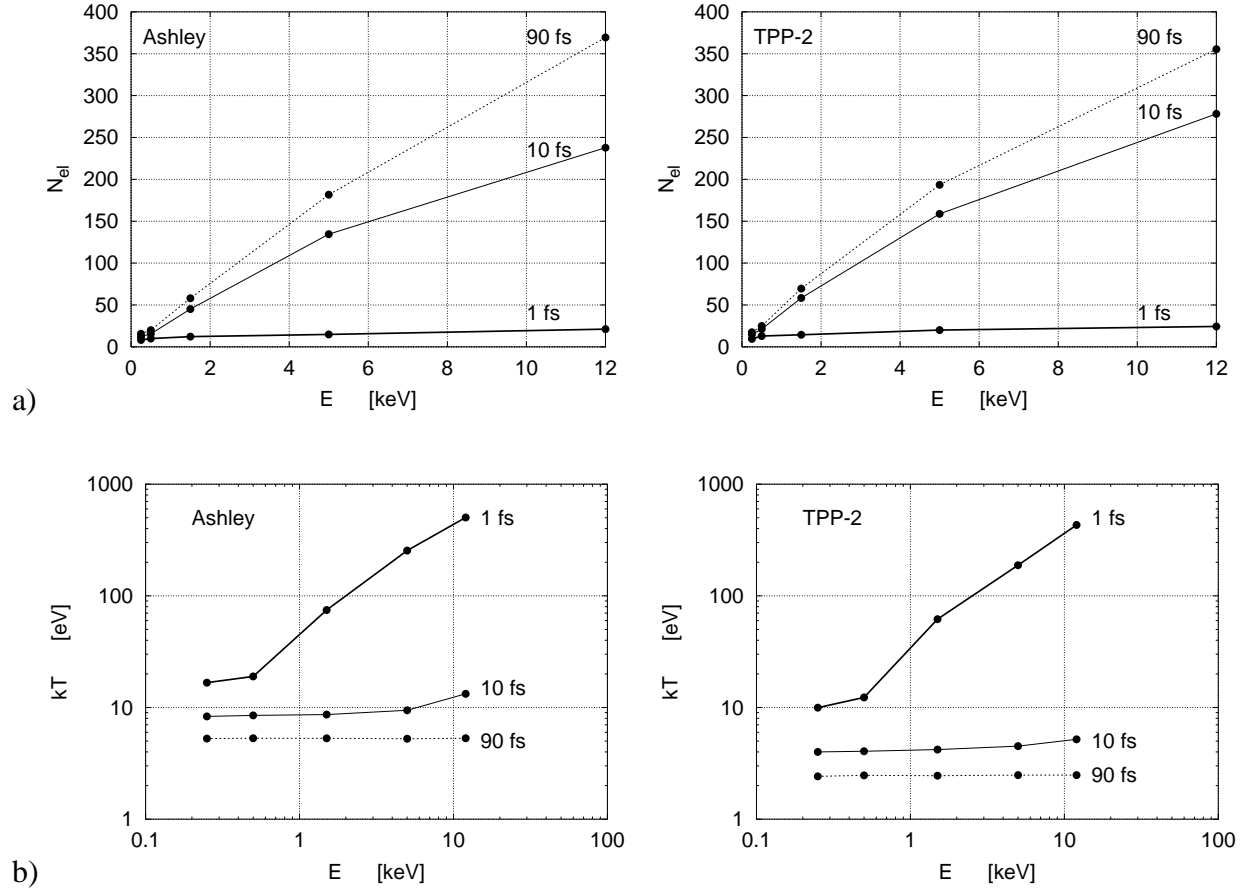


Figure 5: **(a)** Average number of secondary electrons emitted, N_{el} , vs. energy, E ; **(b)** The equivalent instantaneous temperature kT of electron gas vs. energy, E averaged over 500 cascades. Curves correspond to the results obtained at different times $t = 1; 10; 90$ fs from Ashley's model and the TPP-2 model with **no** energy transfer allowed to the lattice. The data were collected at primary energies of $E = 0.25; 0.5; 1.5; 5; 12$ keV. The results at energy $E = 0.25$ keV were taken from [2]

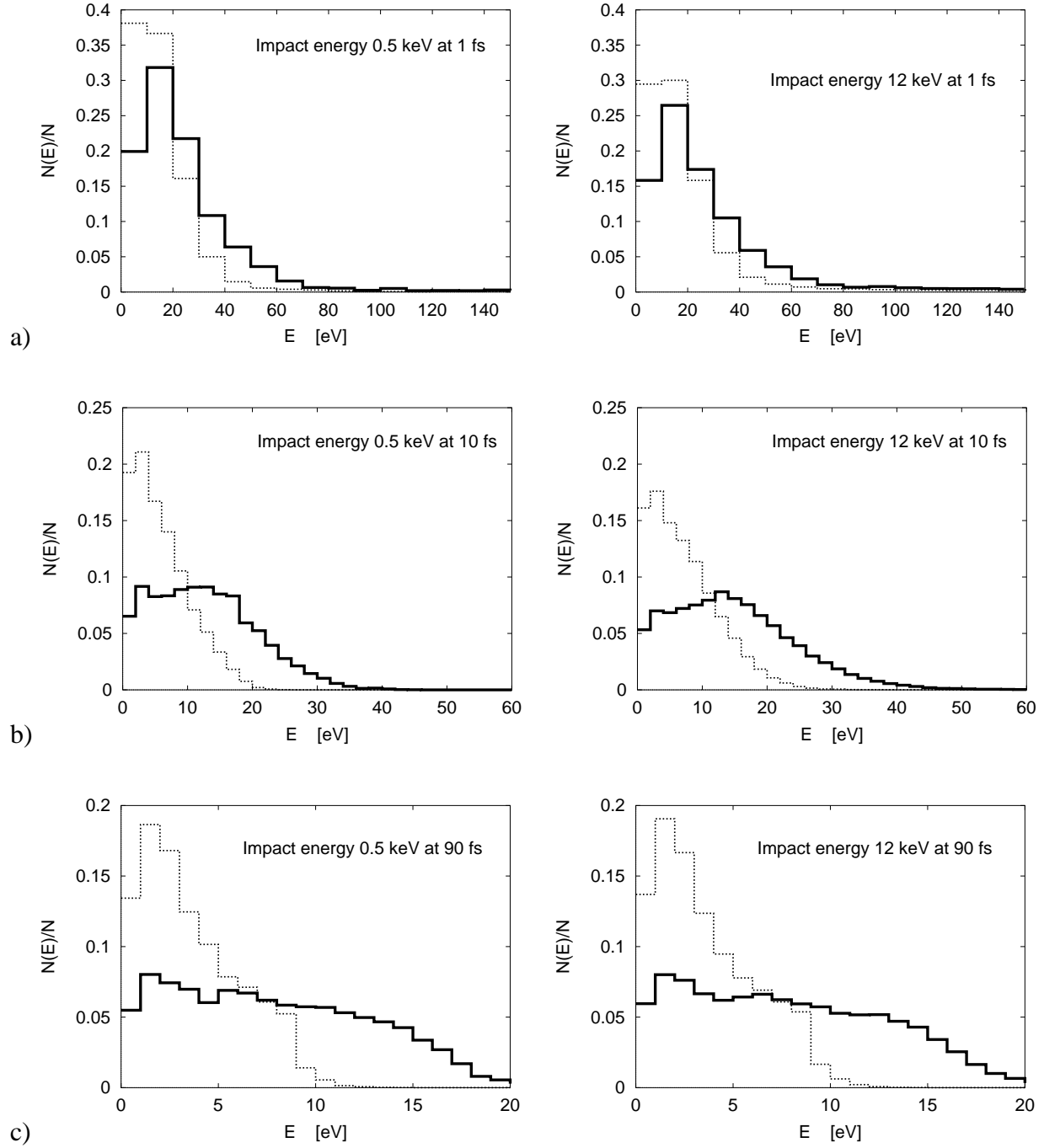


Figure 6: Energy distribution, $N(E)/N$, (fraction of electrons per bin) among electrons (histogram) at **(a)** $t = 1$ fs; **(b)** $t = 10$ fs; and **(c)** $t = 90$ fs. Histograms correspond to results obtained at electron impact of $E = 0.5$ keV (left) and $E = 12$ keV (right) from Ashley's model (solid line) and the TPP-2 model (dotted line) when **no** energy transfer to the lattice is allowed.

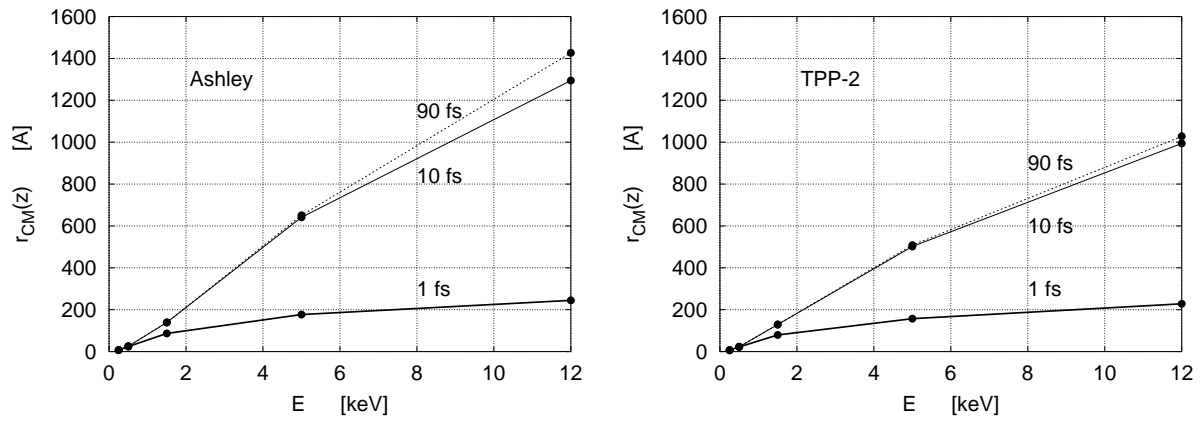


Figure 7: Shifts of the center of mass of the cloud in the direction of the primary impact (Z-axis) vs. energy, E , in respect to the point of emission of the primary impact. Data on the electron cloud were collected from 500 cascades. Curves correspond to the results obtained at different times $t = 1; 10; 90$ fs from Ashley's model and the TPP-2 model with **no** energy transfer allowed to the lattice at primary energies of $E = 0.5; 1.5; 5; 12$ keV.

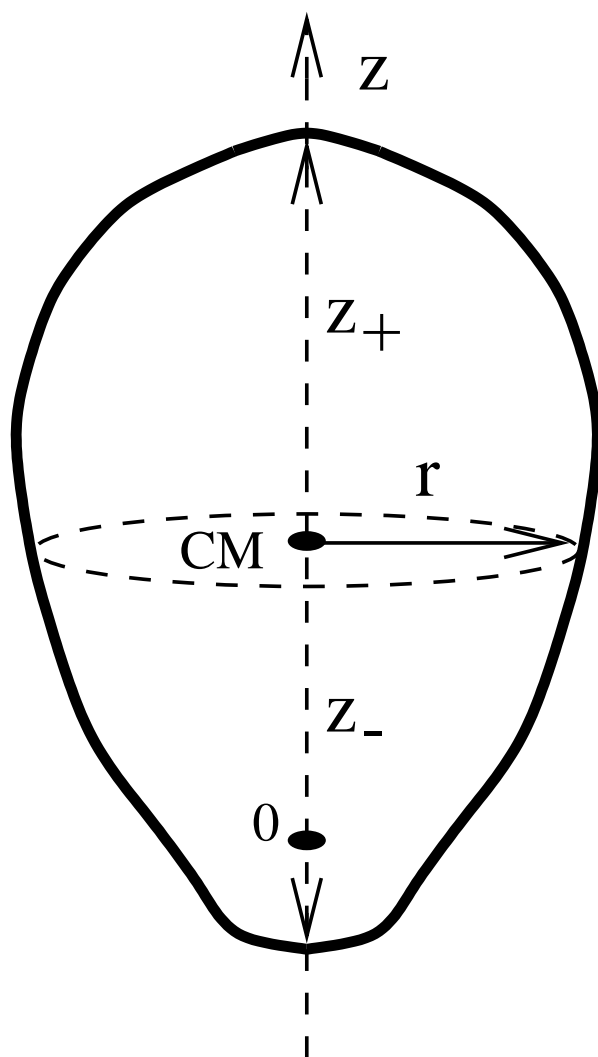


Figure 8: Schematic plot of the electron cloud.

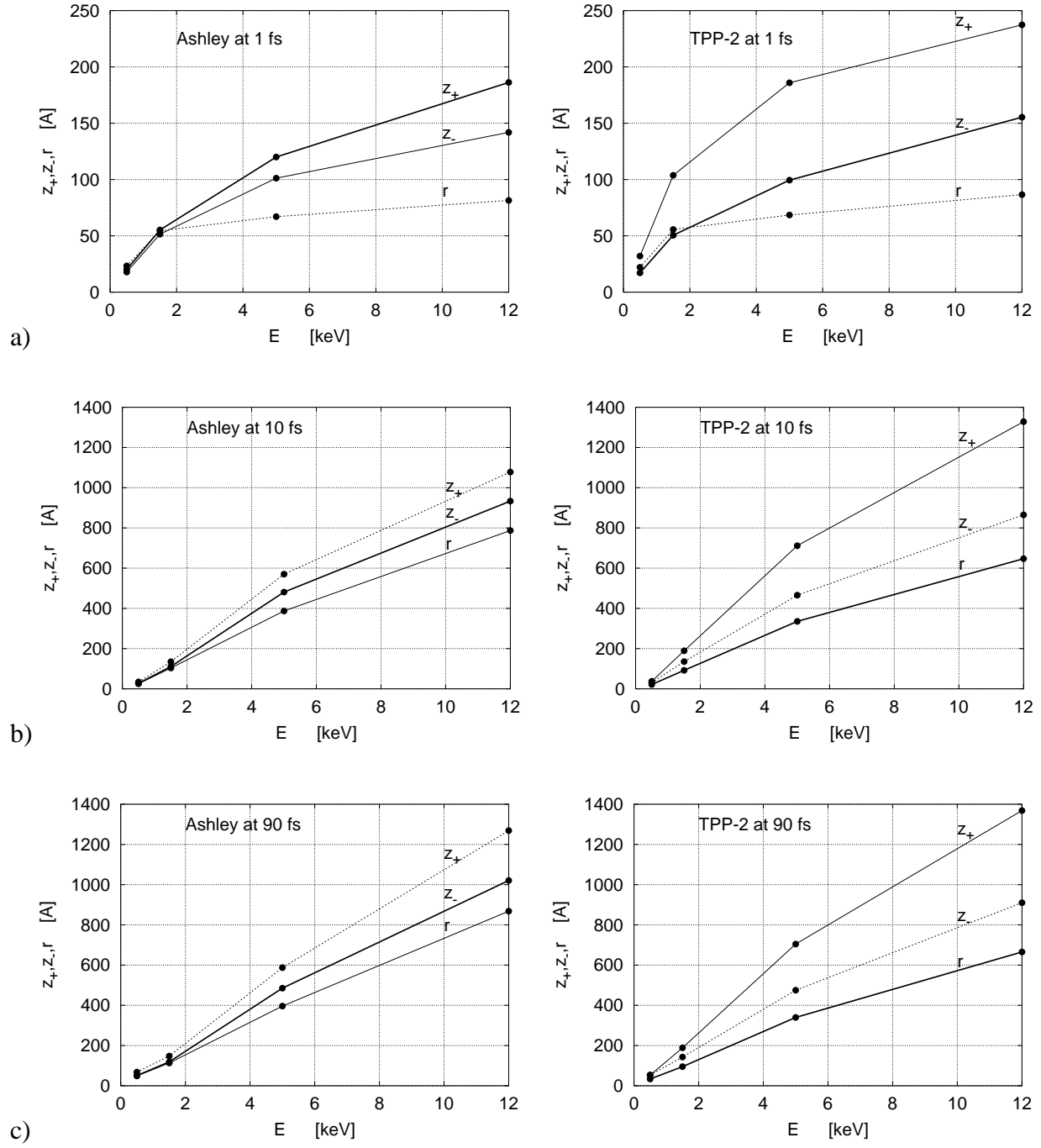


Figure 9: Parameters z_+ , z_- and r describing the spatial structure of the electron cloud. The data from 500 cascades were collected at times: (a) $t = 1$ fs, (b) $t = 10$ fs, (c) $t = 90$ fs at primary energies of $E = 0.5; 1.5; 5; 12$ keV from Ashley's model and the TPP-2 model with **no** energy transfer allowed to the lattice.